Electronic Supplementary Material (ESI) for Nanoscale.

Supporting information

In situ surface hydrogenation synthesis of Ti^{3+} self−doped TiO_2 with enhanced visible light photoactivity

*Junchao Huo, Yanjie Hu**, *Hao Jiang* and *Chunzhong Li**

Key Laboratory for Ultrafine Materials of Ministry of Education, School of Materials Science and Engineering, East China University of Science & Technology, Shanghai 200237, China

Corresponding authors: czli@ecust.edu.cn (C. Z. Li) and huyanjie@ecust.edu.cn (Y. J. Hu)

Fax: +86 21 64250624. Tel: 86- 21- 6425- 0949.

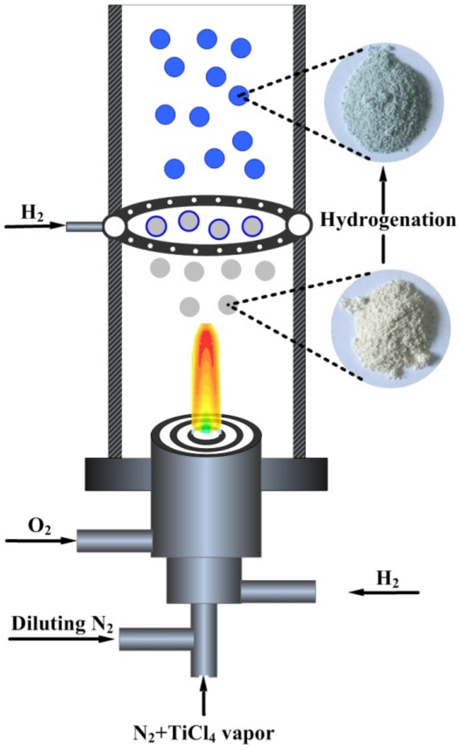

Fig. S1.Schematic setup for Ti^{3+} self–doped TiO_2 nanoparticles

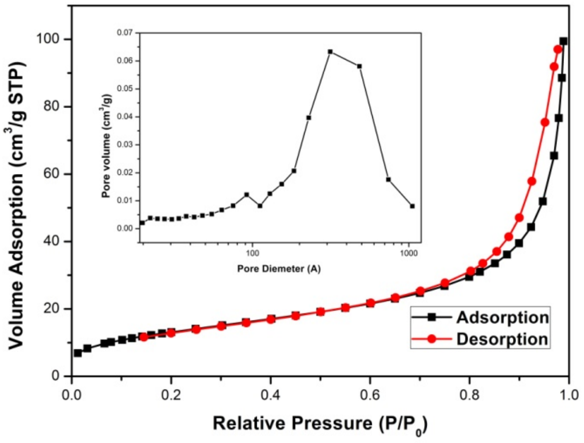

Fig. S2. Nitrogen adsorption-desorption isotherms and corresponding pore size distribution of Ti^{3+} self-doped TiO_2

Fig. S2 shows the nitrogen adsorption-desorption isotherms of the Ti^{3+} self-doped TiO_2 together with the BJH analysis of desorption isotherms in the inset. The isotherm is of type IV (BDDT classification) with a hysteresis loop, which is typical for mesoporous materials. Herein, the presence of mesopores is most likely the result of the aggregation of primary nanoparticles. The BET surface area of the sample is 42.3 m^2/g, and the total pore volume is 0.118 cm^3/g.

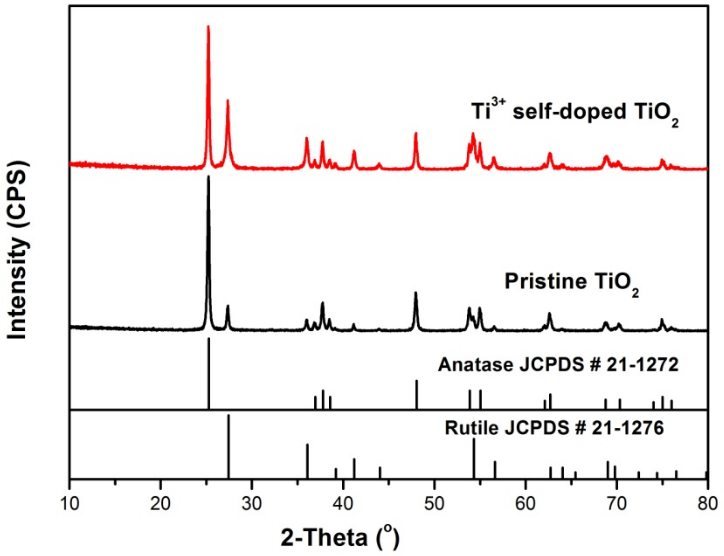

Fig. S3. XRD patterns of pristine TiO_2 and Ti^{3+} self-doped TiO_2

Fig. S3 shows the XRD patterns of TiO_2 without hydrogenation and Ti^{3+} self-doped TiO_2 nanoparticles, suggesting that the samples have good crystalline nature. All diffraction peaks can be indexed to the anatase TiO_2 (JCPDS No. 21-1272) and rutile TiO_2 (JCPDS No. 21-1276), respecting the samples are both mixture of annatase TiO_2 and rutile TiO_2. However, the anatase fraction of Ti^{3+} self-doped TiO_2 nanoparticles (68.7%) is lower than that of TiO_2 without hydrogenation (91.2%). This is because of the introducing of hydrogen increases the reaction temperature above the flame, accelerates the transformation of anatase TiO_2 to rutile TiO_2. The disordered layer observed in the HRTEM image near the surface is not relevant to the increase of rutile phase[1-3]. The average crystallite sizes of Ti^{3+} self-doped TiO_2 nanoparticles are calculated from the anatase (101) and rutile (110) with the Scherrer equation, and are found to be 5.0 nm and 7.8 nm, respectively.

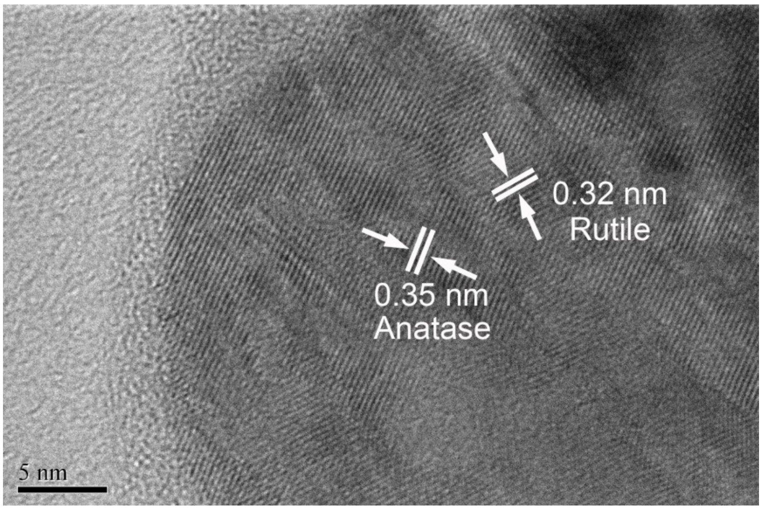

Fig. S4 HRTEM image of Ti^{3+} self-doped TiO_2 with mixture phase

The HRTEM image of Ti^{3+} self-doped TiO_2 with mixture phase is shown in Fig. S4. The mixture of different crystal lattice can be clearly observed, indicating the sample is mixture of annatase TiO_2 and rutile TiO_2, in agreement with XRD patterns.

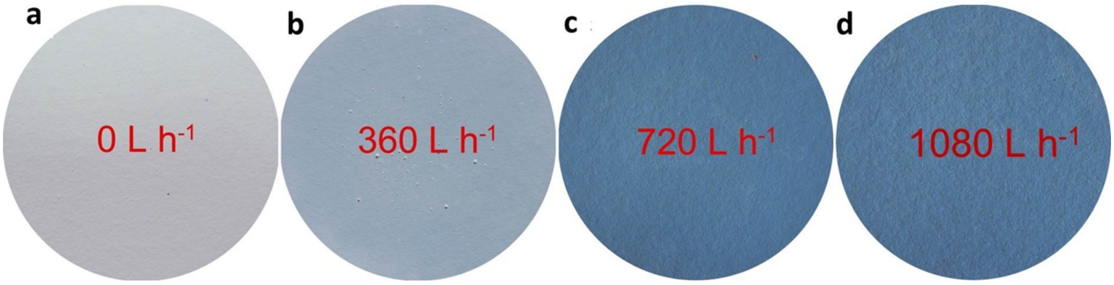

Fig. S5 The different color of Ti^{3+} self-doped TiO_2 with different flow rate of hydrogen, (a) 0 L h^{-1}, (b) 360 L h^{-1}, (c) 720 L h^{-1}, (d) 1080 L h^{-1}

The color can be changed by using different amount of H_2 for hydrogenation (Fig. S5). White products were obtained when none hydrogenation H_2 was used. Light blue and dark blue products can be prepared if 360 L h-1 and 720 L h^{-1} hydrogenation H_2 was used, respectively. Obviously, when the total flow rate hydrogenation H_2 was lower than 720 L h^{-1}, the blue color was much darker as more hydrogenation H_2 was used. However, when the total flow rate hydrogenation H_2 was higher than 720 L h^{-1}, as shown in fig S3d, the blue color almost did not changed when more hydrogenation H_2 was used. This is because while excessive H_2 was used, the mount of H_2 was not the main element influencing the degree of hydrogenation. Therefore the concentration of Ti^{3+} can be modified by the flow rate of hydrogenation H_2.

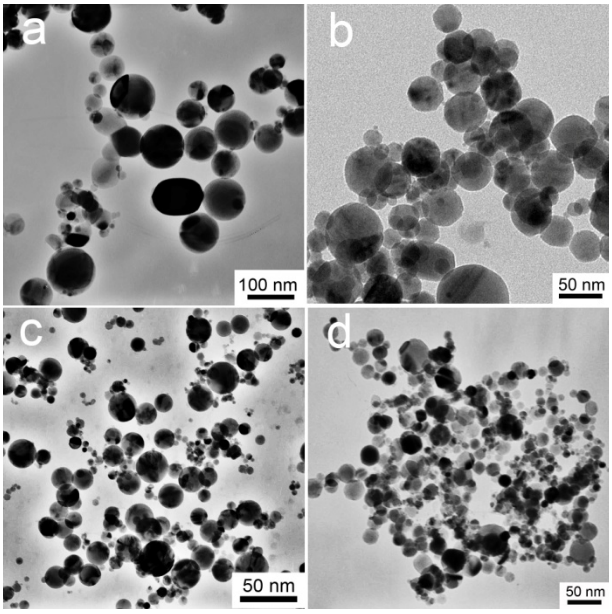

Fig. S6. pore size distribution of Ti^{3+} self-doped TiO_2 with different flow rate of carrier gas. (a) 80 L h^{-1}, (b) 40 L h^{-1}, (c) 20 L h^{-1}, (d) 10 L h^{-1}.

The morphology of obtained samples is found depended on some experimental parameters, the concentration of $TiCl_4$ is the most important parameter. Fig. S6 shows TEM images of samples obtained at different $TiCl_4$ concentration while keeping all of the other conditions constant. The diameter can be decreased by reducing the $TiCl_4$ concentration. When different flow rate (80 L/h, 40 L/h, 20L/h, 10 L/h) of carrier gas of N_2 was used, TiO_2 nanoparticles with average diameter of 70 nm, 40 nm, 20 nm and 15 nm were formed, respectively. However, the obtained TiO_2 using 10 L/h of carrier gas was more uniform, take into the consideration of production rate, 40 L/h of carrier gas was used in our experiment.

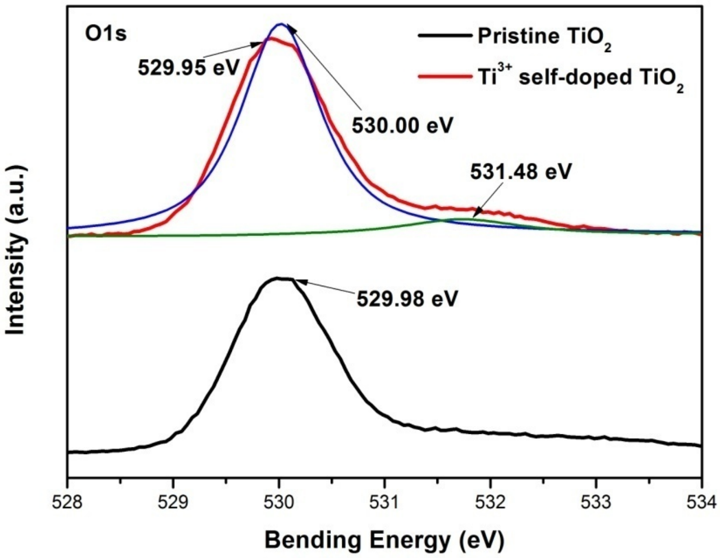

Fig. S7. High resolution XPS spectrum of O_{1s} Ti^{3+} self-doped TiO_2 and pristine TiO_2 without hydrogenation

The O 1s XPS spectra are shown Fig. S7, the signal centered at 529.98 eV and 531.48 eV are the typical signals of Ti–O–Ti and surface OH species, respectively. The O 1s spectra illustrate that Ti^{3+} self-doped TiO_2 has much more surface OH species.

The photodegradation of MB in aqueous solutions using Ti^{3+} self–doped TiO_2, pristine TiO_2 and P25 as photocatalysts with irradiation of ultraviolet light is shown in Fig. S8. The pristine TiO_2 exhibits the best photoactivity under ultraviolet light. The Ti^{3+} self–doped TiO_2 sample exhibits the lowest photoactivity under ultraviolet light. The introduction of H_2 enhanced the temperature of reaction room, accelerated the transformation of anatase TiO_2 to rutile TiO_2. The anatase fraction of Ti^{3+} self–doped

TiO_2 nanoparticles is 68.7%, much lower than that of P25 (79.4%) and pristine TiO_2 (91.2%). The activity of anatase TiO_2 is higher than that of rutile TiO_2, so the photoactivity of Ti^{3+} self–doped TiO_2 sample under ultraviolet light is worse than P25 and pristine TiO_2.

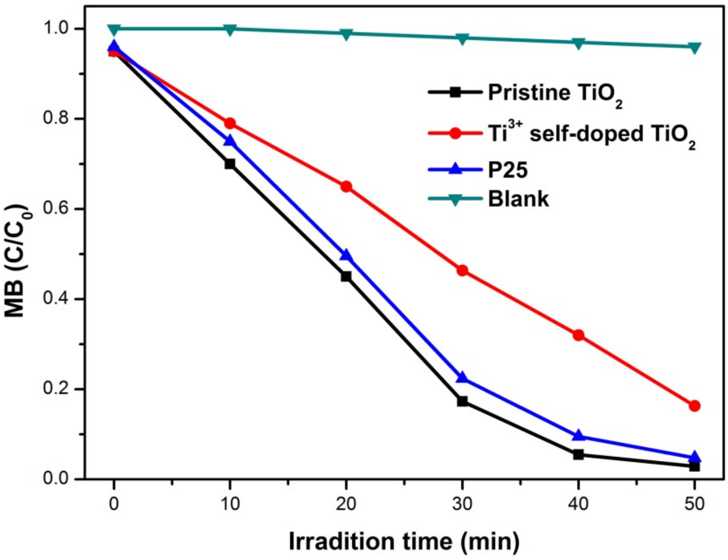

Fig. S8 Photodegradation of MB in aqueous solutions using Ti^{3+} self–doped TiO_2, pristine TiO_2 and P25 as photocatalysts with irradiation of ultraviolet light.

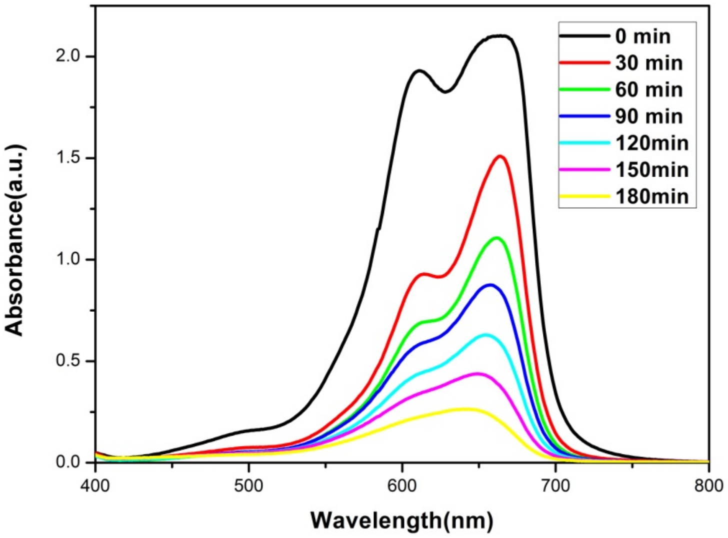

Fig. S9 UV–vis spectrum of MB aqueous solutions in different times by using Ti^{3+} self-doped TiO_2 as photocatalysts under visible light irradiation

1. D. A. H. Dorian, C. C. Sorrell, J Mater. Sci., 2011, **46**, 855.
2. B. F. Xin, H. Wang, J. Wu, R. H. Zhao, Y. F. Lu, B. F. Xin, Appl. Surf. Sci., 2014, **294**, 36.
3. K. Sabyrov, V. Adamson, L. Penn, CrystEngComm, 2014, **16**, 1488.